CELL BIOLOGY

Designer, injectable gels to prevent transplanted Schwann cell loss during spinal cord injury therapy

Laura M. Marquardt[1,2], Vanessa M. Doulames[2], Alice T. Wang[1], Karen Dubbin[1], Riley A. Suhar[1], Michael J. Kratochvil[1,3], Zachary A. Medress[2], Giles W. Plant[2]*, Sarah C. Heilshorn[1]*

Transplantation of patient-derived Schwann cells is a promising regenerative medicine therapy for spinal cord injuries; however, therapeutic efficacy is compromised by inefficient cell delivery. We present a materials-based strategy that addresses three common causes of transplanted cell death: (i) membrane damage during injection, (ii) cell leakage from the injection site, and (iii) apoptosis due to loss of endogenous matrix. Using protein engineering and peptide-based assembly, we designed injectable hydrogels with modular cell-adhesive and mechanical properties. In a cervical contusion model, our hydrogel matrix resulted in a greater than 700% improvement in successful Schwann cell transplantation. The combination therapy of cells and gel significantly improved the spatial distribution of transplanted cells within the endogenous tissue. A reduction in cystic cavitation and neuronal loss were also observed with substantial increases in forelimb strength and coordination. Using an injectable hydrogel matrix, therefore, can markedly improve the outcomes of cellular transplantation therapies.

INTRODUCTION

Spinal cord injury (SCI) is a debilitating condition that currently has no regenerative-based therapy available in the clinic. SCI results in substantial financial, physical, and emotional burdens for patients and their families. Cell-based therapies have emerged as a promising approach to encourage regeneration and functional recovery after SCI (*1*). The transplantation of autologous human Schwann cells (SCs) is currently being investigated in U.S. Food and Drug Administration clinical trials for patients with thoracic and cervical level SCI (*1–4*). SCs are glial cells found in the peripheral nervous system that promote axon regeneration after peripheral nerve injury. Over the past two decades, several preclinical studies have demonstrated that SCs have tremendous potential to promote regeneration after SCI when delivered directly into the lesioned cavity that forms after injury (*4*, *5*). Compared to possible SCI regenerative therapies with pluripotent cells, SCs are highly pure, well characterized, and relatively easy to isolate and expand from the patient's sural nerves (*2*). In addition, the autologous nature of patient-derived SCs removes the need for immunosuppressant drugs compared to allogeneic cell therapies (*6*).

Unfortunately, direct local injection of SCs into the SCI results in significant transplanted cell loss and death (*7*). During injection, typically up to 60% of cells fail to even reach the target site (*8*). This may be due to a combination of factors, including cell membrane damage during injection and cell reflux out of the spinal cord (*8–10*). In addition, previous studies have shown that significant transplanted cell death rapidly occurs as early as 10 min after injection, leading to poor long-term SC survival. Typically, only ~20% of cells survive at 1 week and less than ~5% of transplanted SCs survive 1 month after transplantation, which may correlate with the often mixed functional results observed with SC therapies (*7*, *8*, *11*, *12*). Because SC

retention has been correlated with decreased SCI cavitation and symptomatic relief (*5*, *13*), we hypothesized that increasing the number of transplanted viable cells early after delivery would markedly improve therapeutic efficacy. However, due to limited transplantation volume in the SCI lesion, simply increasing the number of injected cells is not feasible.

In this study, we sought to use a bioengineered injectable material strategy to address three key challenges that hinder SC survival during SCI transplantation (Fig. 1A). During cell delivery, cell loss is caused by (i) cell membrane damage due to extensional forces during injection and (ii) cell dispersal caused by reflux and leakage out of the SCI lesion. Shortly after injection, cell survival is further challenged by the (iii) lack of extracellular matrix (ECM) within the lesion, leading to anoikis, i.e., apoptosis of the anchorage-dependent SCs (*14*). Thus, for transplanted cells to be able to interact with the surrounding endogenous tissue and promote long-term repair, the cells must first overcome these three critical challenges (*5*). Here, we report a shear-thinning, injectable hydrogel that rapidly self-heals to significantly improve the survival and therapeutic function of transplanted SCs as a combination therapy for the treatment of SCI.

RESULTS

SHIELD: An injectable, recombinant protein hydrogel for SC delivery

Three distinct features were designed into our hydrogel materials to address the three critical challenges of transplanted cell survival described above: (i) thixotropy to protect the cell membrane from damage during injection, (ii) rapid self-healing and stiffening in situ to localize the cells within the SCI lesion, and (iii) cell-adhesive ligands to promote SC attachment and spreading. Previous reports by us and others have demonstrated that thixotropic hydrogels that undergo plug-flow fluid mechanics can shield encapsulated cells from damaging mechanical forces during injection (*9*, *15*, *16*). Furthermore, we reasoned that a thixotropic, physical hydrogel would facilitate ease of surgical use, since cells can be pre-encapsulated within the gel and then injected at any time by simply applying a critical yield

[1]Department of Materials Science and Engineering, Stanford University, Stanford, CA 94305, USA. [2]Department of Neurosurgery, Stanford University School of Medicine, Stanford, CA 94305, USA. [3]Division of Infectious Diseases, Stanford University School of Medicine, Stanford CA 94305, USA.
*Corresponding author. Email: gplant@stanford.edu (G.W.P.); heilshorn@stanford.edu (S.C.H.)
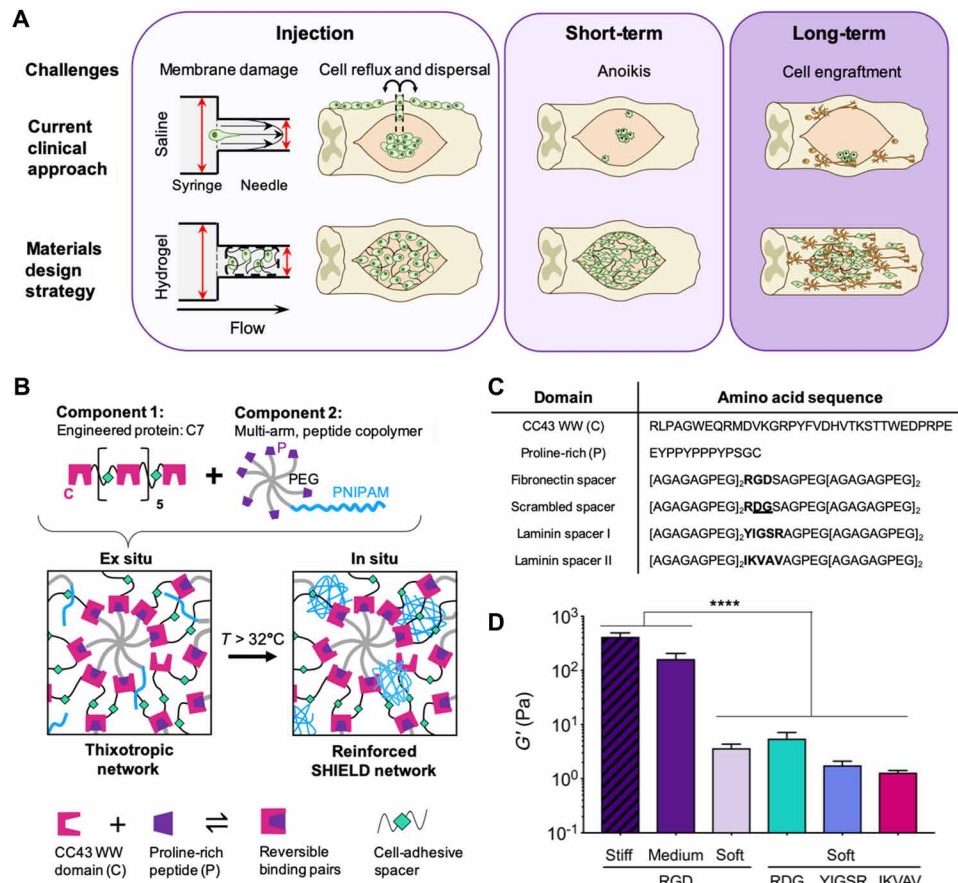
Fig. 1. Materials-based strategy to address the challenges of SC transplantation in SCI. (**A**) Schematic depicting three key challenges SCs face during the transplantation process: (i) membrane damage from extensional forces exerted during syringe needle injection, (ii) cell extrusion and dispersal from the SCI cavity injection site, and (iii) apoptosis due to loss of endogenous matrix. (**B**) SHIELD, an injectable gel designed to address these challenges in cell delivery. Component 1 is C7, a recombinant, engineered protein composed of seven repeats of CC43 WW domains (denoted as C) separated by hydrophilic spacers containing cell-adhesive peptides. Component 2 is a multi-arm, peptide copolymer, 8-armed PEG tethered with proline-rich peptides (denoted as P) and the thermoresponsive polymer (PNIPAM). (**C**) Amino acid sequences of SHIELD components: CC43 WW domain (C), proline-rich peptide (P), and the different cell-adhesive spacer variants. (**D**) Shear storage moduli of soft, medium, and stiff SHIELD formulations with RGD, RDG, YIGSR, and IKVAV cell-adhesive spacers. Data are means ± SEM. ****$P < 0.0001$ statistical significance, Tukey post hoc test. $n = 3$ to 8.

stress to induce flow. In contrast, previous work with fibrin-based gels and other chemically cross-linked gels require careful timing of the injection procedure to ensure that the material does not prematurely form a gel and clog the injection device (*17–19*). Here, we designed a family of injectable, physical hydrogels for SC transplantation based on our previously reported SHIELD (Shear-thinning Hydrogel for Injectable Encapsulation and Long-term Delivery) strategy (*15*). These materials are composed of two components that engage in two stages of cross-linking. The first stage occurs ex situ in which physical cross-links are formed between an engineered recombinant protein (C7) and a multi-arm, polyethylene glycol (PEG)–poly(*N*-isopropylacrylamide) (PNIPAM) copolymer conjugated with proline-rich peptides (P) (Fig. 1, B and C, and fig. S1). These two components assemble ex situ via reversible, heterodimeric binding of two peptide domains (a CC43 WW domain and a proline-rich peptide) to form a weak gel with encapsulated SC (*20, 21*). When the gel is subjected to a force, the peptide-peptide bonds are disrupted, allowing the material to shear-thin and flow as a liquid. After the force is removed, the peptide-peptide bonds rapidly reform, allowing the gel to quickly self-heal.

The second stage of cross-linking occurs in situ to stabilize and stiffen the gel after injection, thereby preventing cell extrusion and leakage out of the lesion, a common challenge for therapies delivered in saline. At body temperature, which is above the PNIPAM lower critical solution temperature of 32°C, the polymer undergoes hydrophobic collapse to provide secondary physical cross-linking to stiffen and reinforce the hydrogel network (Fig. 1B) (*15*). The ideal gel stiffness to retain viable, transplanted SCs within the SCI lesion is currently unknown. Therefore, we formulated materials with a range of the thermoresponsive PNIPAM polymer [0, 1.25, and 2.5 weight % (wt %)], resulting in soft, medium, and stiff gels, respectively (plateau shear moduli, G', ~5, 160, and 400 Pa; Fig. 1D and table S1). These materials span the approximate range of reported neural tissue stiffnesses for the SCI lesion (*22*).

SCs are an anchorage-dependent cell type and undergo anoikis when transplanted into an SCI lesion that lacks adhesive ECM proteins. Thus, to promote long-term SC viability, three different cell-adhesive ligands were designed to the spacer domain of the C7 protein (Fig. 1C). Previously, we reported a SHIELD variant that included the fibronectin-derived RGD cell-adhesive ligand for use

in culture of human adipose–derived stem cells (*15*). The RGD epitope is also known to promote SC adhesion and migration; therefore, this same variant was included here (*23*). In addition, laminin is known to be a major component of the neural ECM and is reported to promote SC elongation and migration through F-actin polymerization (*24*–*26*). Therefore, C7 variants including the laminin-derived cell-adhesive ligands known to induce cell spreading and attachment, YIGSR and IKVAV (*27*, *28*), were newly designed and synthesized. To incorporate these ligands into our C7 recombinant proteins, engineered plasmid cassettes were inserted into pET-15b plasmids and transformed into BL21(DE3) pLysS *Escherichia coli*. Proteins were expressed under the T7 promoter, purified by affinity column, and characterized by gel electrophoresis, amino acid analysis, and Western blotting (figs. S2, S3, and S4). As a negative control material, we also cloned, expressed, and purified a C7 variant containing the non–cell-adhesive RDG sequence. As expected, modification of the cell-binding domain did not significantly alter the mechanical properties of the gel (Fig. 1C and fig. S5).

SHIELD provides cell membrane protection to injected SCs

Cells can experience membrane damage when exposed to extensional forces during syringe needle injection (Fig. 1A) (*9*). This is hypothesized to occur even at the very slow flow rates used here for SCI transplantation (500 nl/min), since the magnitude change in linear velocity of the solution is governed by the geometry of the syringe needle device. As the cells pass from the syringe barrel [inner diameter (ID) = 0.485 mm] into an ultra-small needle (33 gauge,

ID = 0.11 mm), the fluid linear velocity increases 20-fold. Previously, we have reported that shear-thinning, self-healing hydrogels can protect many different cell types from membrane damage during syringe needle injection (*15*, *29*, *30*). To evaluate the ability of our designed SHIELD material to protect SCs from cell membrane damage during transplantation, we recreated the injection procedure in vitro using the same injection parameters described in in vivo transplantation studies (Materials and Methods). As expected, when cells are delivered either in saline or a viscous solution of the C7 RGD polymer (5 wt %; fig. S6), a statistically significant fraction of the cells experience acute membrane damage (25 and 20%, respectively, compared to 3% for the no injection control; Fig. 2, A and B). Mixing the C7 RGD polymer with the PEG-P-PNIPAM polymer (both at 5 wt % final concentration) enables creation of a shear-thinning, rapidly self-healing hydrogel (Fig. 2C). As expected, changing the identity of the cell-adhesive ligand or the amount of PNIPAM within the gel formulation did not alter the shear-thinning gel behavior (Fig. 2C and fig. S7). Pre-encapsulating the SCs within these SHIELD variants provided significant cell membrane protection during syringe needle flow (Fig. 2, A and D). Soft, medium, and stiff SHIELD variants all resulted in statistically higher levels of cell protection compared to cell delivery in saline. Similarly, the presence or absence of the RGD cell-adhesive domain within the SHIELD material did not affect the cell membrane protection. Together with the observation that C7 RGD polymer alone is unable to provide protection, these data suggest that the shear-thinning/self-healing properties of the gel (and not the gel cell-adhesive properties) are
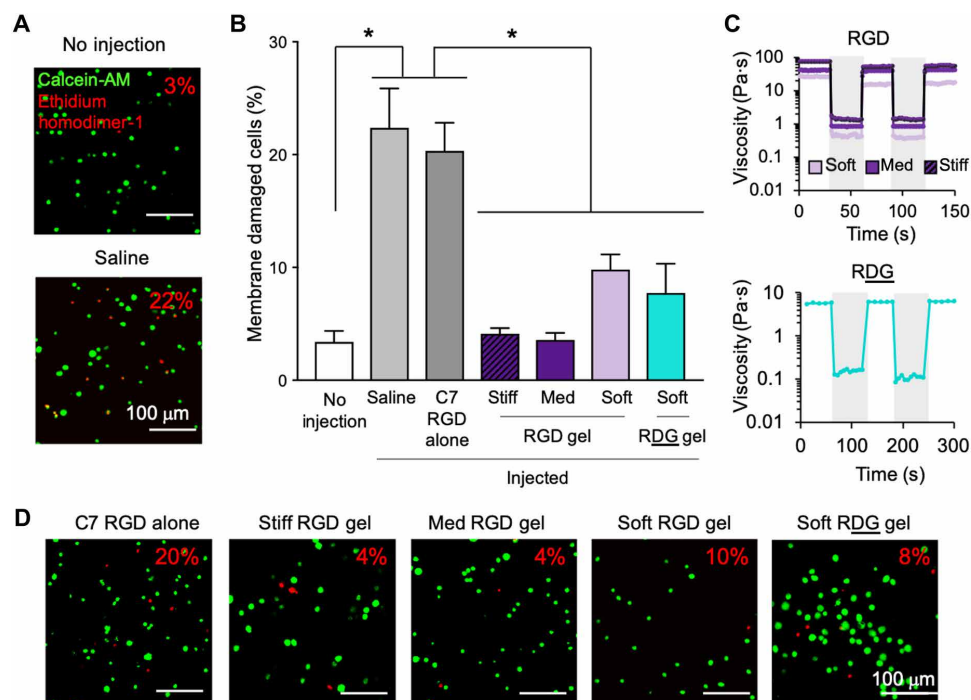

Fig. 2. Thixotropic SHIELD gels provide protection from membrane damage that occurs during syringe needle injection. (**A**) LIVE/DEAD staining confirms that SCs experience significant membrane damage upon exposure to extensional forces as they travel through a syringe needle in saline at 500 nl/min. Green, calcein-AM (live cells); red, ethidium homodimer-1 (dead cells). (**B**) Percentage of SCs with membrane damage when injected in SHIELD gels is significantly lower than those injected in saline or C7 alone, regardless of SHIELD stiffness or cell-adhesive ligand. Data are means ± SEM.*P < 0.05, one-way analysis of variance (ANOVA) with Tukey post hoc test. n = 3 to 16 individual injections, three to seven independent experiments. (**C**) Shear-thinning and self-healing behavior of soft, medium, and stiff SHIELD gels with RGD cell-adhesive ligand and soft RDG SHIELD at 0.1 (*7*) and 10 (gray) Hz. Data are means ± SD. n = 3. (**D**) Representative LIVE/DEAD images of SCs injected at 500 nl/min in a viscous solution of C7 RGD alone; soft, medium, or stiff SHIELD gels with RGD ligands; or soft RDG SHIELD gel.

responsible for the cell membrane protection. To further confirm this idea, SCs were delivered within a comparison hydrogel formed from decellularized basement membrane matrix of a murine Engelbreth-Holm-Swarm sarcoma (commonly known by the trade name Matrigel). As expected, this control hydrogel did not provide statistically significant cell membrane protection (fig. S8).

Hydrogel biomechanical and biochemical properties modulate SC behavior

As SHIELD materials of low, medium, and high stiffness all provided cell membrane protection during injection, these materials were all further evaluated for their ability to support SC culture in vitro. SCs have been reported to respond to the mechanical stiffness of 2D culture substrates by altering their proliferation rate (31); therefore, we first evaluated proliferation in our 3D gels by quantifying total DNA over time. SCs were homogeneously encapsulated as individual, dissociated cells at a density of 1.5×10^7 cells ml^{-1} gel for each cell-adhesive variant (fig. S9). In our stiffest RGD-containing SHIELD formulation, SC DNA content over 3 and 7 days was significantly reduced compared to cells in soft or medium stiffness gels (Fig. 3A). Therefore, this stiffest formulation was excluded from further studies. While DNA content was highest in the medium stiffness RGD SHIELD gel at both 3 and 7 days, the overall SC viability was similarly high (>80%) across all three gel stiffness variants, suggesting that this stiffness range can support SC viability within a three-dimensional (3D) hydrogel context (Fig. 3, A to D, and figs. S9 and S10). Similarly, SC viability was not significantly affected by the choice of cell-adhesive ligand across the entire range of gel stiffness, although complete lack of a ligand (the RDG SHIELD variant) was beginning to trend down in viability at day 7 for soft gels, consistent with the possible initiation of anoikis (Fig. 3, A to D, and fig. S10). Previous reports by others have suggested that SC elongation and migration are dependent on F-actin polymerization, both in vitro and in vivo during regeneration of the peripheral nerve (25, 26). Thus, an ideal hydrogel formulation would promote migration and elongated morphology of transplanted SCs after transplantation. Therefore, we selected to evaluate F-actin polymerization in the different cell-adhesive gel formulations via phalloidin staining. SCs in the RGD SHIELD gels extended significantly longer processes than cells in the RDG, YIGSR, and IKVAV SHIELD gels (Fig. 3, E and F). This SC morphology is an indicator of cell-adhesive ligand engagement with the RGD peptide. While cell processes were observed to extend from SCs in other formulations, these were predominantly found within large cell clusters, potentially indicating a preference for cell-cell contacts and/or self-secreted matrix, rather than interaction with the SHIELD ligands (Fig. 3, E and G). Across all cell-adhesive ligand variants, no statistically significant differences in SC process extension or cell cluster size were observed when comparing between the soft and medium stiffness gels (Fig. 3, E to G). Together, our in vitro SC analysis resulted in the selection of the medium stiffness SHIELD gel with the RGD ligand for continued study. In this SHIELD formulation, SC morphology and expression of normal SC markers P75 and S100 were maintained, supporting its further evaluation as an SC delivery vehicle in a preclinical model of SCI (fig. S9).

SHIELD increases transplanted SC retention and spread morphology

We selected a unilateral, cervical contusion SCI model in female Fischer 344 rats chosen to represent the most commonly encoun-

tered SCI in patients (32). Briefly, a right, 75-kdyne contusion injury was performed at the fifth cervical (C5) level following a dorsal laminectomy (Fig. 4A). After 2 weeks of recovery, which is considered the subacute phase for this SCI model (33), an intended dose of 4.0×10^5 SCs was delivered in either SHIELD (n = 13) or saline (n = 13) using a 33-gauge Hamilton syringe (table S2). Injury only (n = 8) and saline (n = 8) injection served as negative controls. Transplanted SC retention was assessed at 48 hours (N = 10) and 4 weeks (N = 16) after transplantation. Consistent with our in vitro transplantation model data, we observed significantly higher numbers of P75$^+$ cells at the lesion site when delivered in SHIELD compared to saline (Fig. 4D). Transplantation of exogenous, syngeneic SCs was confirmed by labeling cells with Qtracker655 and costaining for P75 (fig. S11), and control animals exhibited no P75$^+$ staining (fig. S12). At 48 hours, 32,000 ± 7700 viable, transplanted cells were observed in animals receiving SHIELD, while 4300 ± 2500 viable, transplanted cells were found in animals receiving saline. Thus, while both cohorts had markedly fewer cells than the initial cell dosage, SHIELD transplantation resulted in a ~740% increase in viable local cell delivery compared to the clinical standard of saline transplantation. At 4 weeks, 29,000 ± 8000 viable cells delivered with SHIELD were observed, while 2400 ± 800 viable cells were counted for the saline-delivered animals, a ~10-fold increase in local delivery of viable cells compared to saline. In spinal cord cross sections at both time points, larger SC transplants were observed for SHIELD delivery compared to saline delivery (Fig. 4E). Consistent with reports by others, in some cross sections, the "track" left by the injection needle is still visible, suggesting that the reflux of saline during needle removal can result in a significant loss of transplanted cells (fig. S13). Together with our in vitro data, these observations suggest that the use of a shear-thinning, self-healing hydrogel can significantly improve SC delivery to the SCI lesion by providing cell membrane protection during injection and limiting cell extrusion from the injection site into the subarachnoid space.

To assess the ability of our SHIELD material to promote cell adhesion in vivo, analysis of SC transplant morphology was performed at 48 hours. Consistent with reports by others, cells delivered in saline remained as compact clusters of spherical cells, indicative of the loss of native matrix within the SCI lesion. In contrast, SCs delivered in SHIELD were significantly more elongated and extended throughout the lesion (Fig. 5A), indicative of cell adhesion to the transplanted material. Cell shape was quantified by the spindle ratio defined as the major axis length divided by the short axis length. Cells in SHIELD had a statistically significant 3.05-fold increase in spindle ratio compared to cells in saline (Fig. 5B). At 4 weeks after transplant, cells delivered in saline were primarily observed near the original site of injection at the C5 level of the spinal cord (Fig. 5C, top). In contrast, SCs delivered in SHIELD were found to extend longitudinally through the cord, in both the rostral and caudal directions (Fig. 5C, bottom). Transplanted cell distribution was quantified by manually counting the number of cells within a 60-μm-thick section at 360-μm intervals. Consistent with our qualitative observations, cells delivered in SHIELD were significantly more spread throughout the cord than those in saline (P = 0.0013, Kolmogorov-Smirnov analysis; Fig. 5D).

Increased SC retention with SHIELD ameliorates secondary injury

It has long been hypothesized that the mechanism of SC action on SCI regeneration and functional recovery occurs through modulating
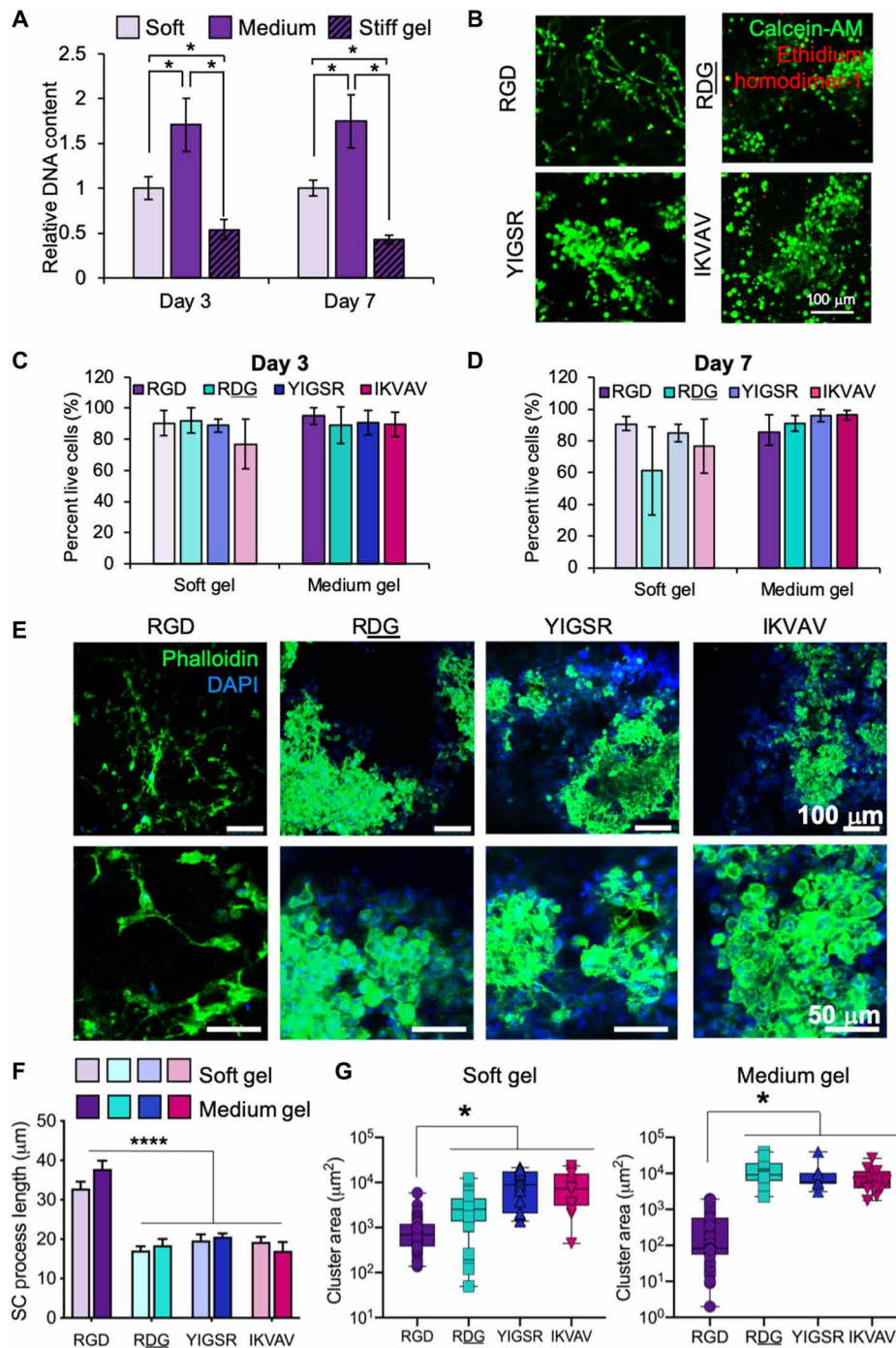
Fig. 3. SC behavior in SHIELD variants with distinct biomechanical and biochemical properties. (**A**) DNA quantification of SCs encapsulated in soft, medium, and stiff RGD SHIELD gels for 3 and 7 days normalized to soft SHIELD gels. Data are means ± SEM. *$P < 0.05$, one-way ANOVA with Tukey post hoc test. $n = 5$ to 6, three independent experiments. (**B**) Representative LIVE/DEAD images of SCs encapsulated in medium stiffness SHIELD gels with varying cell-adhesive ligands after 3 days in culture. Green, calcein-AM (live cells); red, ethidium homodimer-1 (dead cells). (**C** and **D**) SCs display high viability (>80%) across all SHIELD cell-adhesive variants for both soft and medium stiffness gels after 3 days of culture, while at 7 days, SCs in soft SHIELD variants lacking a cell-adhesive ligand (RDG) show increased variability in viability. Data are means ± SEM. No statistical significance, one-way ANOVA with Tukey post hoc test. $n = 2$ independent experiments, each with ≥2 technical replicates. (**E**) Representative fluorescent images of SC morphology in medium stiffness SHIELD gels with varying cell-adhesive ligand domains after 3 days in culture. Green, phalloidin (F-actin); blue, DAPI (4′,6-diamidino-2-phenylindole dihydrochloride; nuclei). (**F**) Quantification of SC process length in soft and medium stiffness SHIELD gels with varying cell-adhesive ligands demonstrates that RGD gels promote significantly longer SC cytoplasmic processes after 3 days in culture. Data are means ± SD. *$P < 0.05$, one-way ANOVA with Tukey post hoc test. $n = 3$ to 11, ≥2 independent experiments. (**G**) Quantification of SC cluster area in soft and medium stiffness SHIELD gels with cell-adhesive variants after 3 days demonstrates significantly larger cell clusters in the RDG, YIGSR, and IKVAV variants. Data are box and whisker plots with mean, min, and max. *$P < 0.05$, one-way ANOVA with Tukey post hoc test. $n = 2$ independent experiments, each with ≥2 technical replicates.
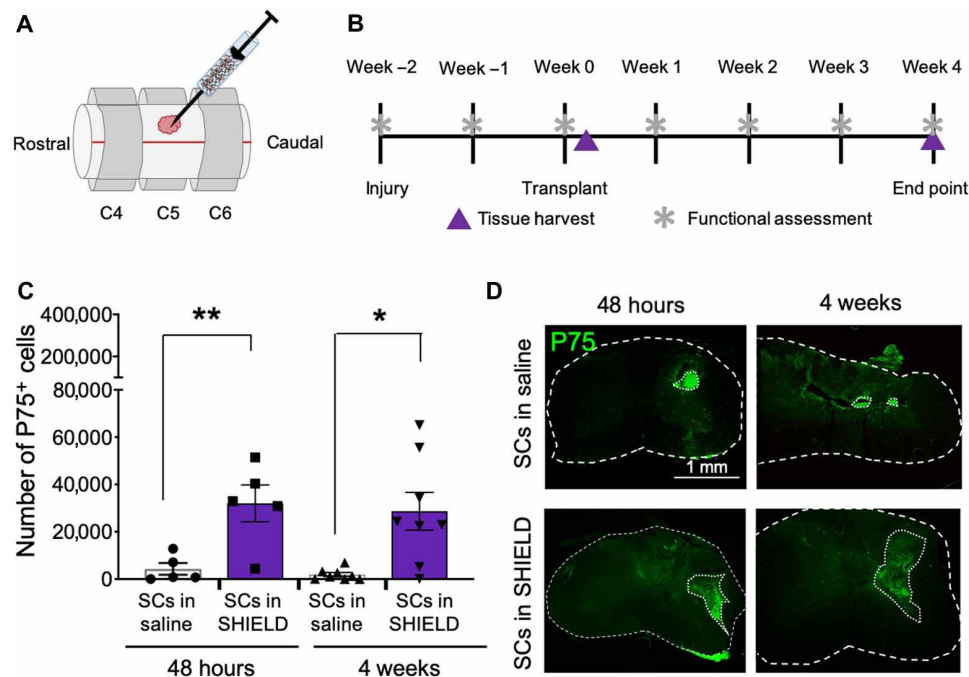
Fig. 4. SHIELD delivery improves short- and long-term SC retention in a rat model of cervical SCI. (**A**) Schematic of SCI model. Following a C5 laminectomy, Fischer rats receive a right 75-kdyne contusion injury. Two weeks later (subacute phase), SCs are transplanted directly at the injury site using an automated syringe needle device. (**B**) Experimental time course of in vivo model of SC transplantation, behavioral assessment, and tissue harvest. SC retention is assessed in spinal cord explants at 48 hours and 4 weeks after transplantation. Behavioral assessments of forearm function are performed before injury, after injury, and weekly following SC transplantation. (**C**) Quantification of the number of P75$^+$ SCs at 48 hours and 4 weeks after transplantation demonstrates significantly higher SC retention when delivered in SHIELD compared to saline. Data are means ± SEM. **$P < 0.01$ and *$P < 0.05$, unpaired, two-tailed t test. $n = 8$ animals, $N = 2$ independent experimental replicates. (**D**) Representative fluorescent images of P75$^+$ cells in spinal cord explants transplanted with SCs in saline or SHIELD at 48 hours and 4 weeks after transplantation.

the secondary injury response within the endogenous tissue, resulting in minimization of cystic cavitation (*5*). Unfortunately, poor transplanted cell survival limits their therapeutic potential to enact this response. Here, we immunostained spinal cord sections with endogenous tissue and cell markers to assess the secondary injury and native tissue response, including the volume of the cystic cavity. To assess the secondary injury that occurs following SCI, we defined the area devoid of cell nuclei and astrocytes as the cystic cavity, the adjacent 100 μm as the lesion, and the subsequent adjacent 100 μm as the peri-lesion (Fig. 6A) (*34*). The total cavitation volume was quantified by measuring the cavity cross-sectional area at 360-μm intervals throughout the entire lesion. Delivering SCs in SHIELD significantly reduced the cystic cavitation volume compared to animals treated with SCs in saline, saline only, and injury only ($P = 0.004$, 0.014, and 0.0329, respectively; Fig. 6B). When comparing the cystic lesion volume in each individual animal to their number of surviving transplanted SCs at 4 weeks (data in Fig. 4C), a statistically significant correlation was observed ($P = 0.0314$, Pearson correlation test, 95% confidence interval). These data are consistent with previously published reports that demonstrate transplanted SCs result in greater tissue sparing (*5*). The glial scar response was quantified by measuring the percentage of area staining positively for reactive astrocytes [glial fibrillary acidic protein (GFAP)] in the adjacent lesion and peri-lesion regions. We found that while all groups had formation of a glial scar, SHIELD delivery of SCs led to a significant reduction in the reactive astrocyte response in the peri-lesion space (Fig. 6C). To quantify the neuronal population within the spinal

cord after injury, we performed βIII-tubulin staining and compared the staining intensity within the injured and uninjured hemispheres (excluding the cavity) to account for interanimal variability (Fig. 6A). While injury only and saline only control animals had a ~0.6 neuronal ratio between the injured and uninjured hemispheres, delivery of SCs in SHIELD had a significantly higher neuronal ratio of ~0.8 ($P = 0.0487$ and 0.0426, respectively; Fig. 6D). This result is consistent with previous reports in which increased SC retention was observed with increased neuronal and axon area (*13*). Because of the timing of this staining (4 weeks), this ratio is likely a measurement of neuronal and axonal sparing and minimization of the secondary injury, rather than axonal regeneration.

We also examined the response of endogenous immune and vascular cells to SC transplantation in saline or SHIELD (Fig. 7). Here, we only observed a significant difference in pan-macrophage (ED1) response in the lesion and peri-lesion areas, where SC delivery in SHIELD appeared to have fewer macrophages within the injury after 4 weeks compared to injury only control animals (Fig. 7A). SCs are known to influence macrophage behavior through paracrine signaling (*35*), and thus, improving the localized survival of SCs has the potential to influence numerous downstream cell signaling processes. However, as we only observe hematogenous macrophage response at this single 4-week time point, future work would need to include multiple time points and cellular identities to characterize the full dynamic response of immune cell infiltration, as much of the early inflammation is often resolved by 4 weeks (*36*, *37*). No differences in lesion and peri-lesion staining were observed for microglia
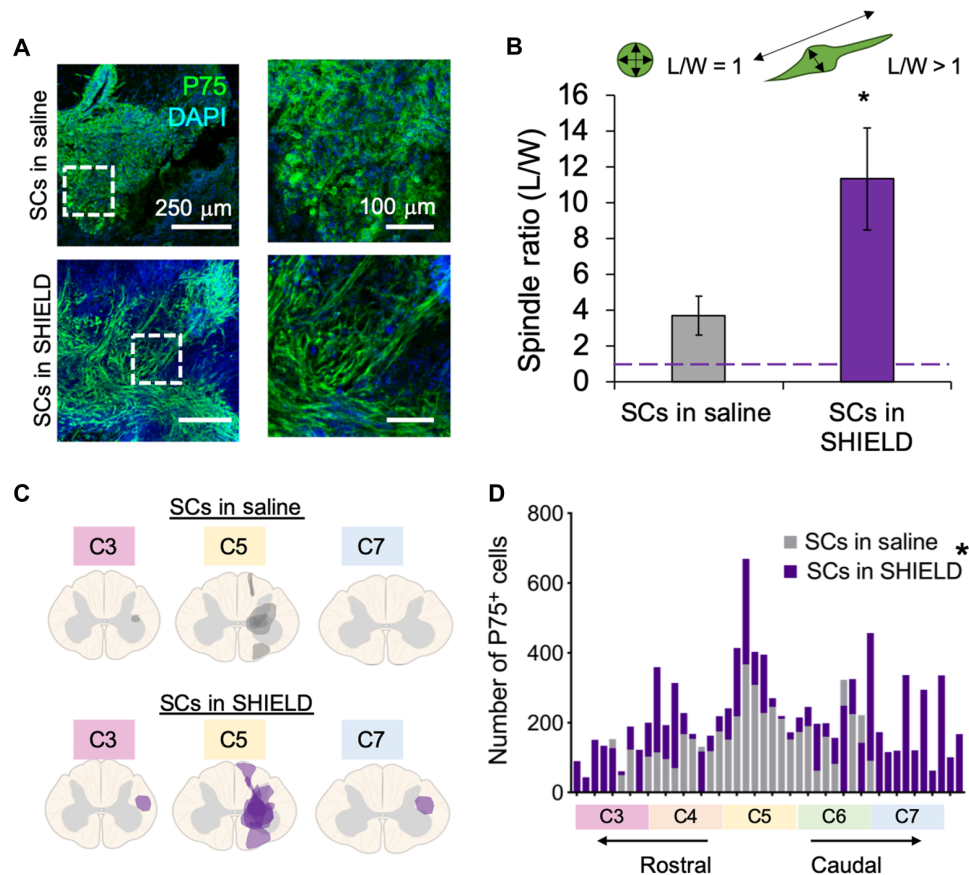
Fig. 5. Transplanted SCs have an extended morphology and greater tissue distribution when delivered in SHIELD. (**A**) Fluorescent images of P75+ SCs 48 hours after transplantation demonstrate significant morphological differences between cells delivered in saline compared to SHIELD. (**B**) Quantification of SC morphology as measured by spindle ratio (major axis/minor axis) demonstrates that SHIELD-delivered SCs are substantially more elongated than saline-delivered cells. Data are means ± SEM. *$P < 0.05$, unpaired t test. $n = 4$ to 5 animals, $N = 2$ independent experimental replicates. (**C**) Distribution of SCs within the spinal cord 4 weeks after transplantation was visualized in histological cross sections as P75+ areas and projected onto the C3 to C7 schematic. SHIELD-transplanted SCs show a greater spatial distribution within the endogenous tissue compared to saline. (**D**) Histogram of P75+ SCs observed throughout the spinal cord within different segments 4 weeks after transplantation shows significantly greater distribution in both the rostral and caudal directions for SHIELD-delivered cells compared to saline. Data are means ± SEM. *$P < 0.05$, Kolmogorov-Smirnov test of cumulative distribution. $n = 4$ to 5 animals, $N = 2$ independent experimental replicates.

(Iba1/Tomato lectin) and vascularization (Tomato lectin) (Fig. 7, B and C). Similarly, no significant differences were observed for each stain (ED1, Iba1, and Tomato lectin) when comparing between the injured and uninjured hemispheres (fig. S14). Together, these results support the idea that increased delivery of SCs to the site of an SCI contusion lesion modulates the secondary injury, resulting in decreased formation of a cystic cavity.

Hydrogel-mediated cell delivery increases functional recovery

SCs have been a therapeutic focus for treating SCI for several decades. Unfortunately, while SCs have been demonstrated to limit cystic cavitation in several preclinical models, the reported functional improvement in these models has often been modest, which we hypothesized to be due to poor viable cell delivery. Therefore, we evaluated the combination cell and injectable hydrogel therapy on functional forelimb recovery. Both motor and sensorimotor tests were performed to obtain a more complete picture of right forelimb function, as contusive SCI can result in both motor and sensory deficits (32, 38). To assess forelimb motor recovery, we measured

forelimb grip strength (39, 40). Both combined and right arm strength were evaluated to assess whether left arm compensation influences the right arm behavior. As anticipated, unilateral C5 contusion results in both combined and right forelimb grip strength deficit, although the reduction is significantly greater in right forearm only tests (Fig. 8, A and B). Over the experimental period, no group reached pre-injury level; however, in both combined and right forelimbs, we observed a significant increase in grip strength for animals treated with SCs in SHIELD compared to injury only controls ($P = 0.0295$ and 0.0114, respectively; Fig. 8, A and B). Furthermore, right forelimb grip strength for SCs in SHIELD-treated animals was significantly higher than saline only and SCs in saline ($P = 0.0138$ and 0.0165, respectively; Fig. 8, A and B). No significant improvement was observed for the animals treated with SCs in saline. We also assessed the sensorimotor recovery of animals through the Horizontal Ladder Walk test (41). This assay measures forelimb coordination by counting the number of forearm missed steps (complete and partial) as the animal traverses a horizontal ladder with unevenly spaced rungs. As anticipated, we observed a significant increase in missed steps after cervical contusion SCI (Fig. 8C). At 4 weeks after
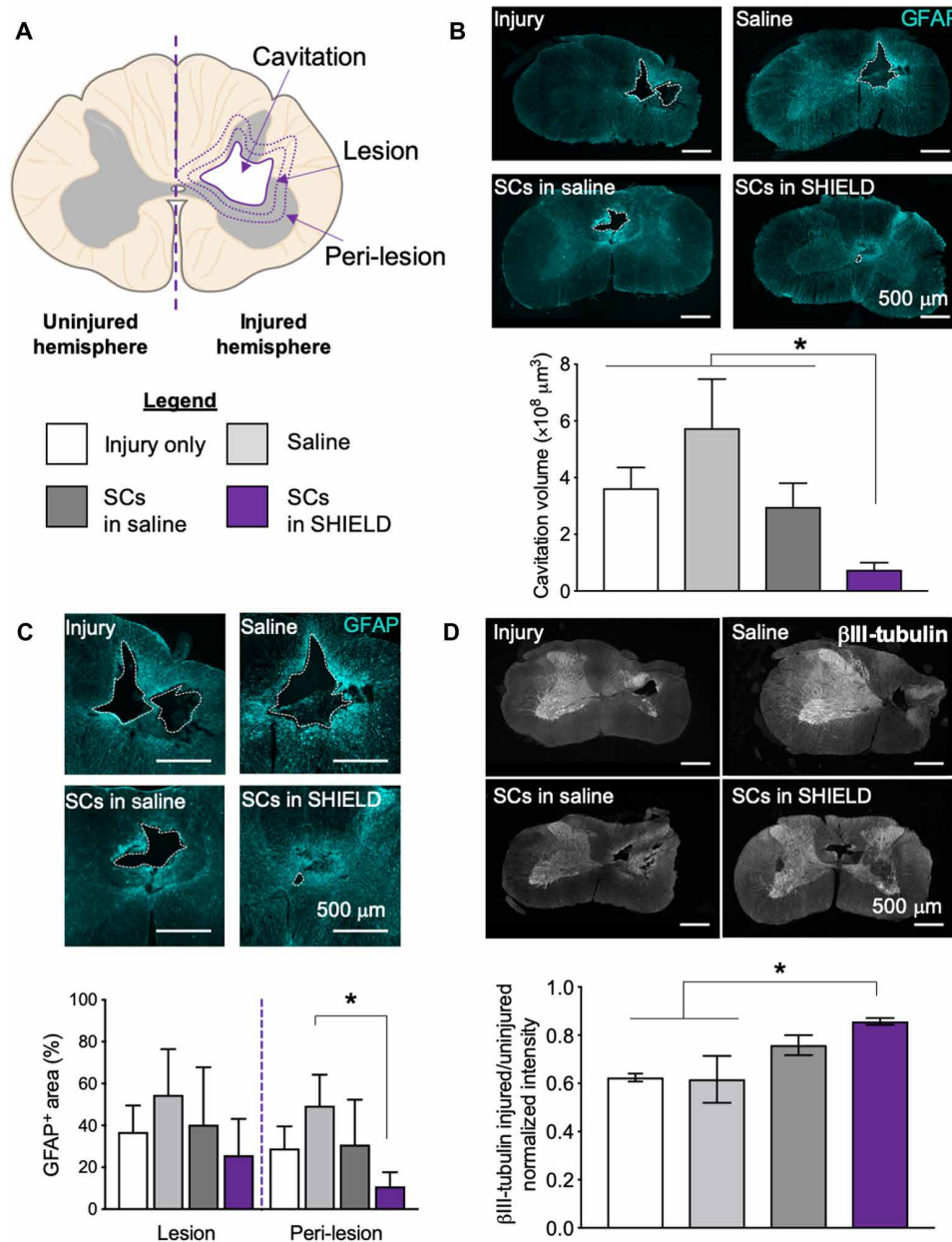
Fig. 6. SC delivery with SHIELD minimizes the secondary injury response. (**A**) Schematic of secondary injury characterization in spinal cord sections delineating the cystic cavitation, the adjacent lesion and peri-lesion areas, and uninjured and injured hemispheres. (**B**) Representative whole scan fluorescent images of spinal cord sections display cavity areas across all groups. Cyan, GFAP. Quantification of cavitation volume shows significantly smaller cavities in animals treated with SCs delivered in SHIELD. Data are means ± SEM. *$P < 0.05$, one-way ANOVA, unpaired t test post hoc analysis. $n = 7$ to 8, $N = 2$ independent experiments. (**C**) Glial scar formation is a hallmark of SCI and can be observed by increased GFAP staining surrounding the cystic cavity. Cyan, GFAP. Quantification of GFAP-positive area across all groups reveals a decrease in the peri-lesion region of SHIELD-delivered SCs compared to saline only injection. Data are means ± SEM. *$P < 0.05$, one-way ANOVA with Tukey post hoc test. $n = 5$ to 6, $N = 2$ independent experiments. (**D**) Representative fluorescent images of βIII-tubulin–stained spinal cord explants reveal diminished neuronal presence in the injured hemisphere. Normalized injured to uninjured βIII-tubulin intensity demonstrates significantly increased neuronal staining in animals treated with SCs in SHIELD compared to injury only and saline-injected groups. Data are means ± SEM. *$P < 0.05$, one-way ANOVA with Tukey post hoc test. $n = 3$, $N = 2$ independent experiments.

transplant, animals treated with SCs in SHIELD saw a significant decrease in missed steps compared to injury and saline only animals. As with the forelimb strength test, no significant improvement was observed for animals treated with SCs in saline ($P = 0.713$; Fig. 8C). Furthermore, at 4 weeks after transplant, animals treated with SCs in SHIELD only missed $16.62 \pm 1.63\%$ of steps, which was a

significant improvement compared to their post-injury behavior ($35.27 \pm 1.77\%$, $P = 0.0038$) and statistically similar to their pre-injury behavior ($13.81 \pm 0.06\%$, $P = 0.970$). In comparison, animals with injury only, saline only treatment, or transplantation of SCs in saline had statistically negligible improvement from their post-injury behavior ($P = 0.966$, 0.723, and 0.373, respectively). When comparing
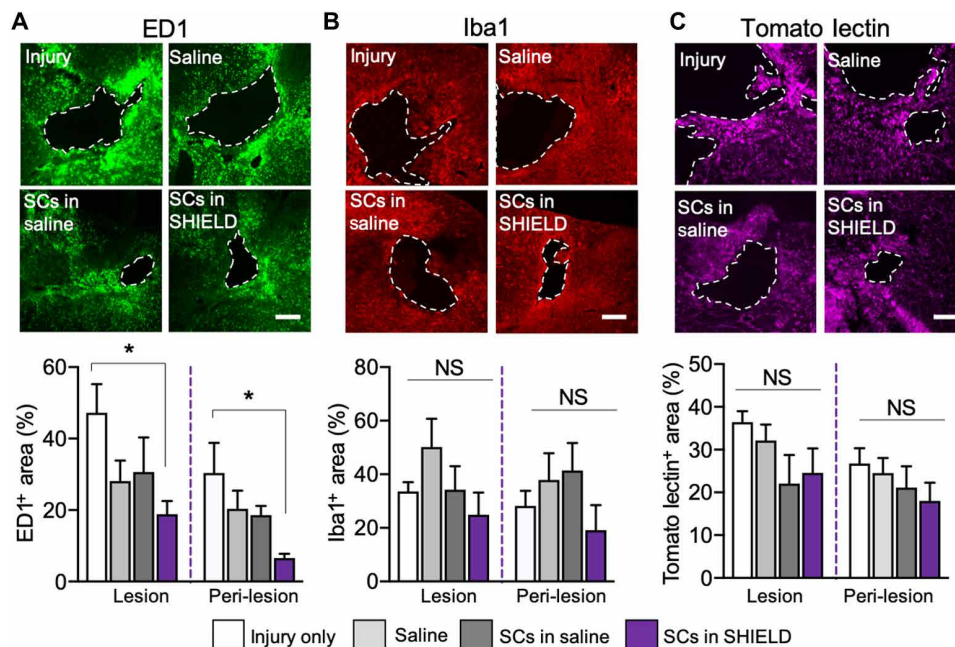
Fig. 7. SHIELD delivery of SCs modulates the endogenous tissue response that follows SCI. (**A**) Representative fluorescent images of immunostained spinal cord sections for pan-macrophage marker, ED1. Quantification of ED1$^+$ area revealed statistically decreased staining in the lesion and peri-lesion regions for animals receiving SCs in SHIELD compared to injury only controls. Data are means ± SEM. *$P < 0.05$, one-way ANOVA with Tukey post hoc test. $n = 7$ to 8, $N = 2$ independent experiments. (**B** and **C**) Representative fluorescent images of immunostained spinal cord sections for microglia (Iba1) and vasculature (Tomato lectin). Quantification revealed no significant differences in (B) Iba1 and (C) Tomato lectin staining in the lesion and peri-lesion regions across the groups. Data are means ± SEM. $n = 3$ to 8, $N = 2$ independent experiments. NS, not significant.

the functional outcome in each individual animal to their number of surviving transplanted SCs at 4 weeks (data in Fig. 4C), a statistically significant positive correlation was observed between the SC count and the combined forelimb grip strength, while a negative correlation was observed between the SC count and the percentage of missed steps in the horizontal ladder assay ($P = 0.0135$ and 0.0068, respectively, Pearson correlation test, 95% confidence interval). No statistically significant correlation was observed between SC count and right forelimb grip strength ($P = 0.1207$), likely due to the high individual variability in the right grip strength measurement. Together, these data are consistent with previously published reports and support our hypothesis that an improvement in the number of successfully transplanted SCs can improve therapeutic outcomes (*5*).

DISCUSSION
Successful delivery of transplanted cells and maintenance of cell viability after transplantation are common challenges faced by many cell-based therapies (*7, 17, 42, 43*). As the dosage and retention of delivered viable cells have been correlated with symptomatic outcomes for a variety of injury and disease models, the inability to successfully transplant cells directly into damaged tissue is a significant hurdle for clinical translation of many potential regenerative medicine therapies (*42–46*). Here, we specifically address the challenge of SC delivery for SCI through the design of a novel biomaterial strategy. SCs are currently in clinical trials for the treatment of SCI, owing to their ability to reduce the secondary injury response (cystic cavitation, glial scar formation, and neuronal loss) that occurs after injury in preclinical models. Unfortunately, due to limited survival

of the transplanted cells and poor localization to the target site, SCs have yet to demonstrate their full potential in improving functional, behavioral recovery. Various approaches to combat transplanted cell death have been explored in the past, often focusing on the codelivery of drugs (i.e., soluble apoptosis inhibitors), growth factors, and/or genes (*11, 47, 48*). While potentially beneficial, this approach requires careful attention to the spatial and temporal delivery of the proper dosage of prosurvival factors to be successful. When the location, timing, and dosage are not precisely controlled and optimized, delivery of these factors has the potential to impede therapeutic efficacy and even, in some cases, cause further functional deficits (*49–51*).

Therefore, to move cell-based therapies toward clinical translation, we proposed an alternative strategy that does not require the careful spatiotemporal dosing control that is associated with small molecules, growth factors, and gene therapies. Our approach improves cell survival by designing a combination cell-plus-hydrogel therapy that addresses three key underlying causes of cell loss: (i) membrane damage during injection, (ii) cell reflux away from the injection site, and (iii) anoikis due to loss of endogenous matrix. While other hydrogel materials have been studied to improve the retention of viable cells, these systems often only address a single cause of cell loss during transplantation and/or rely on the use of a decellularized matrix from Engelbreth-Holm-Swarm murine sarcoma (often known by the trade name Matrigel), which is not clinically translatable (*13, 52, 53*). Other natural-based materials have been investigated for improving SC transplantation, including an acellular, injectable peripheral nerve matrix; however, many of these materials suffer from batch-to-batch variability that can limit the reproducibility of the
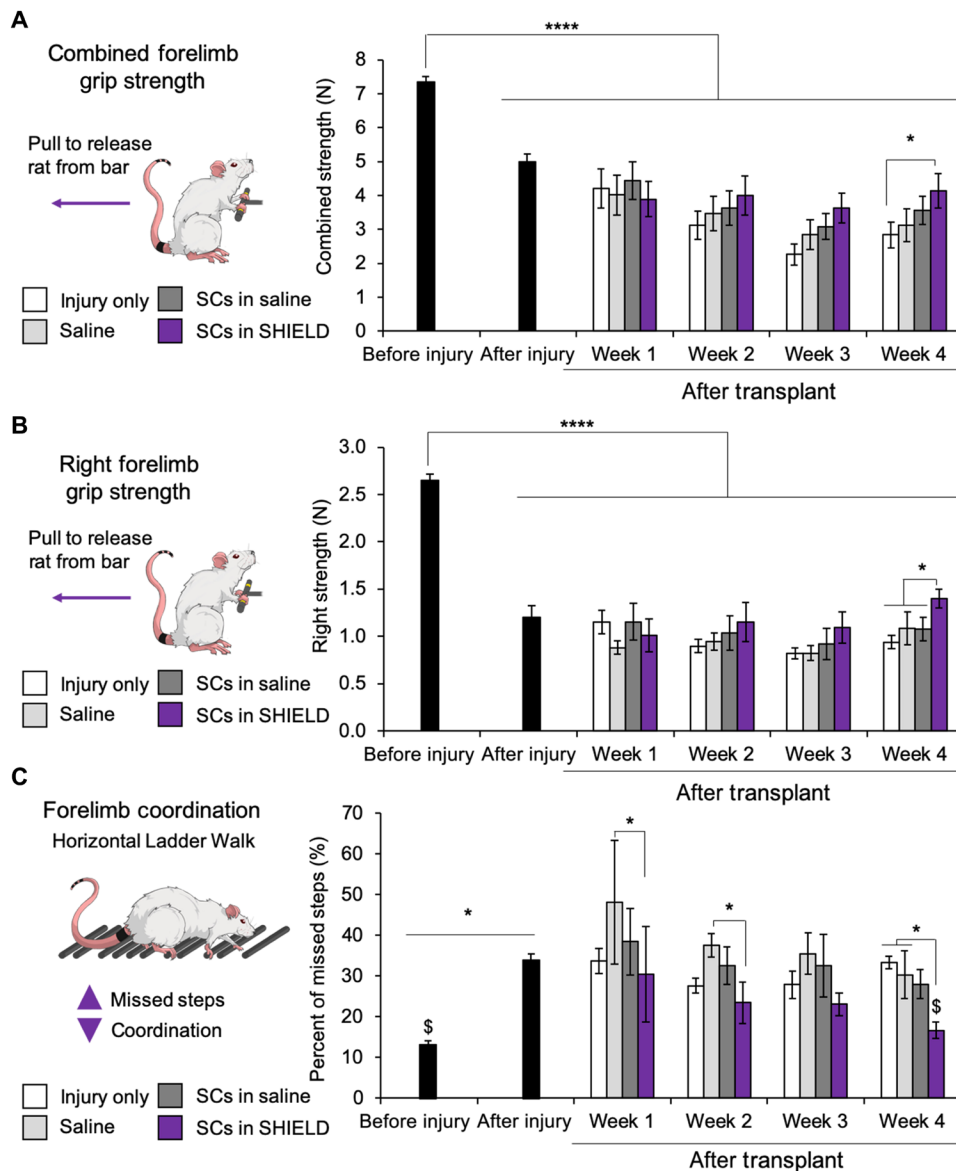
Fig. 8. Significant forelimb recovery is achieved with SHIELD delivery of SCs after SCI. Forearm motor and sensorimotor function was assessed before injury, after injury, and weekly after transplantation using a grip strength meter (A and B) and Horizontal Ladder Walk test (C), respectively. (**A**) Combined forearm grip strength significantly decreases following SCI. By 4 weeks after transplantation, grip strength was significantly increased in animals treated with SCs in SHIELD compared to injury only animals. (**B**) Relative to combined forearm grip strength, quantification of right forearm strength alone results in a more pronounced deficit due to the right, unilateral contusion injury. However, similar to combined forearm strength, by 4 weeks, right forearm grip strength is significantly increased over injury only controls. Data are means ± SEM. ****$P < 0.0001$ and *$P < 0.05$, one-way ANOVA with Tukey post hoc test. $n = 47$ before injury, $n = 53$ after injury, $n = 7$ to 8 after transplantation, $N = 2$ independent experiments. (**C**) Forelimb coordination was assessed with the Horizontal Ladder Walk test; after injury, a decrease in coordination presents as an increase in missed steps. Four weeks following SC transplantation in SHIELD, a significant decrease in percentage of missed steps is observed compared to injury only control animals. In addition, SC delivery in SHIELD results in a similar percentage of missed steps to that of pre-injury levels. Data are means ± SEM. *$P < 0.05$ and $$P = 0.970$ comparison between before injury and 4-week SCs in SHIELD, one-way ANOVA with Tukey post hoc test. $n = 37$ before injury, $n = 53$ after injury, $n = 7$ to 8 after transplantation, $N = 2$ independent experiments.

SC response (*54*). In contrast, our designed gel material, SHIELD, contains three mechanisms of action within a single material that results in a greater than 700% increase in transplanted SC survival compared to the clinical standard of saline delivery. In addition, the biomechanical and biochemical properties of SHIELD were designed to not only increase cell number but also improve transplanted cell function by providing a 3D, cell-adhesive, physical support with

ECM cues selected to enhance F-actin polymerization and elongated cell morphology, which has been correlated with SC migration in vitro and in vivo during regeneration of the peripheral nerve (*25, 26, 55*). The use of SHIELD to improve the successful transplantation of SCs resulted in a significant reduction in the secondary injury and pronounced increases in forelimb strength and coordination after SCI, thereby demonstrating functional efficacy. Moreover,

our designed material platform is fully chemically defined for rigorous reproducibility and future evaluation by regulatory agencies.

While we report a significant improvement in cell retention compared to the clinical standard of saline delivery, cell loss from initial injection number does occur using our material platform. This result indicates that additional optimization can be undertaken to further improve cell survival by using the modular design of the hydrogel system for a complete and systematic interrogation of combinations of biochemical ligands. As biochemical ligands can often have nonlinear synergistic and antagonistic effects, these future studies would likely require computational algorithms to assist in identifying the optimal ligand formulation, as has been previously reported for other cell types (56, 57). In addition, in the scope of this study, we report the use of a combination cell-plus-hydrogel therapy on spinal regeneration and functional recovery. However, further investigation of our designer, injectable hydrogel alone is of considerable interest, as material alone may potentially have endogenous effects, as reported for other injectable materials (58, 59). These future experimental opportunities for continued material optimization highlight the potential of our platform not only for use in SCI but also for numerous other clinical indications that suffer from similar limitations. Last, while our study was focused on the use of a designer hydrogel platform for SCs, as they are currently in clinical trials, our study has broader implications for use of other cell types in treating SCI. The modular nature of this hydrogel system would enable easy customization for alternative cell types and for other clinical indications beyond SCI where the successful transplantation of cell-based therapies is critical for therapeutic efficacy.

MATERIALS AND METHODS
Synthesis and characterization of SHIELD hydrogels
SHIELD component synthesis
SHIELD hydrogels are physically cross-linked, two-component hydrogel systems composed of (i) a recombinant engineered protein termed C7 and (ii) a synthetic 8-arm PEG polymer modified with proline-rich peptides (P) and the thermoresponsive polymer, PNIPAM. The recombinant C7 proteins were designed to contain seven repeats of the CC43 WW protein binding domain interspaced with six repeats of selected cell-adhesive domains (RGD, RDG, YIGSR, and IKVAV; see fig. S2 for full amino acid sequences) (20). C7s were expressed in BL21(DE3)pLysS *E. coli* (Life Technologies) based on a previously published procedure (21). Briefly, C7s were cloned into pET-15b plasmids and expressed under control of the T7 promoter. Bacteria containing the plasmids were cultured in Terrific broth to an OD_{600} (optical density at 600 nm) of 0.8, and expression was induced by 1 mM isopropyl β-D-1-thiogalactopyranoside. After 24 hours, the bacteria were harvested by centrifugation, resuspended in lysis buffer [10 mM tris, 1 mM EDTA, and 100 mM NaCl (pH 8.0)], and lysed by multiple freeze-thaw cycles. Lysates were treated with deoxyribonuclease I and 1 mM phenylmethanesulfonyl fluoride protease inhibitor. The C7 variants were purified by affinity chromatography via the specific binding of an N-terminal polyhistidine tag to Ni-nitrilotriacetic acid resin (Qiagen), dialyzed against phosphate-buffered saline (PBS), and concentrated by diafiltration across Amicon Ultracel filter units (Millipore). Protein purity was confirmed by SDS–polyacrylamide gel electrophoresis (SDS-PAGE), Western blotting, and amino acid sequencing. Expressed protein was separated by SDS-PAGE, transferred to a polyvinylidene difluoride membrane,

blocked with nonfat milk, and probed with 6×HisTag (Cell Signaling Technology) primary antibody. The primary antibody was detected using horseradish peroxidase–conjugated secondary antibody (1:10,000; donkey anti-rabbit, Jackson ImmunoResearch). Blots were developed with SuperSignal West Pico or Femto Chemiluminescent Substrates (Pierce) and imaged using a ChemiDoc MP gel imaging system (Bio-Rad). Before use for any in vivo transplantation studies, C7 was endotoxin-purified using previously published protocols (60). Briefly, endotoxin was removed from the C7 solution using thermocycling in a 1% Triton X-114 solution. Triton X-114 was then removed from the solution using Bio-beads SM-2 Resin (Bio-Rad).

PEG-P and PEG-P-PNIPAM were synthesized according to previously published protocols (15, 30). Briefly, 8-arm PEG vinyl sulfone (8-arm PEG-VS) with a nominal molecular weight of 20 kDa was purchased from Nanocs (Boston, MA). Peptide P (EYPPYPPPPYPSGC, 1563 g/mol) was purchased through custom peptide synthesis from GenScript Corp. (Piscataway, NJ, USA). All other chemicals were purchased from Sigma-Aldrich (Milwaukee, WI) unless otherwise noted. PNIPAM endcapped with a thiol group (PNIPAM-SH) (molecular weight, 30 kDa) was synthesized using reversible addition–fragmentation chain transfer polymerization and conjugated to the 8-arm PEG-VS via a Michael-type addition reaction according to previously published protocol. The stoichiometry of the PNIPAM conjugation reaction was altered to modify, on average, either 0.5 or 1 arm of the PEG-VS as confirmed by ^{1}H nuclear magnetic resonance (NMR) (fig. S1). Unreacted arms of PEG-VS were further reacted with excess P peptide in the presence of tris(2-carboxyethyl)phosphine (Sigma-Aldrich, St. Louis, MO). The stoichiometry of the P conjugation reaction was altered to modify, on average, 7 arms of the PEG-VS as confirmed by ^{1}H NMR (fig. S1). The PEG-P-PNIPAM copolymer solution was lyophilized, washed with chloroform to remove unreacted PEG, and then dialyzed (molecular weight cutoff, 3 kDa) against deionized water (pH 7.4) to remove unreacted PNIPAM and P. For comparison, PEG-P copolymer was synthesized by reacting 8-arm PEG-VS with excess P and purified as described above. Once again, the P conjugation reaction was confirmed by ^{1}H NMR (fig. S1).

SHIELD gel fabrication
SHIELD gels were prepared by adding appropriate amount of PBS to reach a 10% (w/v) C7 and a 10% (w/v) PEG-P or PEG-P-PNIPAM solution. For gel fabrication, each WW domain in C7 was treated as one C unit, and each pendant P peptide group in the PEG-P-PNIPAM copolymer was treated as one P unit and components were mixed to achieve a C:P ratio of 1:1 and final polymer concentration of 10% (w/v). To fabricate the three different SHIELD mechanical formulations (soft, medium, and stiff), appropriate amounts of 10% (w/v) PEG-P and/or PEG-P-PNIPAM were added to the 10% (w/v) C7 solution for a final 10% polymer solution with 0, 1.25, and 2.5% final PNIPAM concentrations (table S1). The final concentration of cell-adhesive peptides in each hydrogel is estimated to be 6.5 mM.

SHIELD rheological characterization
Dynamic oscillatory rheology experiments were performed on a stress-controlled rheometer (AR-G2, TA Instruments, New Castle, DE) using a 25-mm-diameter cone plate geometry. Samples were loaded immediately onto the rheometer after mixing, and a humidity chamber was secured in place to prevent dehydration. Frequency sweeps from 0.1 to 10 Hz at 25° and 37°C were performed at 1% constant strain to obtain storage moduli (G') and loss moduli (G''). Shear-thinning and self-healing properties of the gel samples were characterized by measuring viscosity (η) under a time sweep mode

at alternating low and high shear rates of 0.1 and 10 s^{-1}, respectively, for 60 s each and a total of 300 s.

Cell culture

Primary adult SCs were isolated from micro-dissected sciatic nerves of 8- to 10-week-old syngeneic female Fischer rats following a protocol approved by the Stanford Administrative Panel on Laboratory Animal Care. The National Institutes of Health (NIH) guidelines for the care and use of laboratory animals were observed (NIH publication no. 85–23 Rev. 1985). SCs were expanded in growth medium [Dulbecco's modified Eagle's medium (DMEM), fetal bovine serum, GlutaMAX, Antibiotic-Antimycotic (ABAM) (Life Technologies), pituitary extract (20 μg/ml; Gibco), and 2 μM forskolin (Sigma)] on poly-L-lysine–coated tissue culture plastic following a previously described protocol (fig. S8) (12). SCs were used between passages 2 and 4 for all in vitro and in vivo studies. To obtain pure (>90%) SC cultures from any contaminating endogenous endoneurial fibroblasts, SCs were separated on the AutoMACs (Miltenyi Biotec) using the Possel D2 software setting and the low-affinity nerve growth factor receptor p75 [supernatant 192-IgG (immunoglobulin G)] and mouse IgG magnetic microbeads (Miltenyi).

In vitro injection studies

For in vitro cell injection studies, SCs were lifted by trypsinization, pelleted, resuspended, and counted. The SCs were pelleted again and resuspended in the different delivery materials to achieve a final cell density of 2.5×10^7 cells ml^{-1}. This cell density was selected to maximize the number of individual injection replicates that could be performed per independent round of study. SCs were encapsulated in 4 μl of SHIELD hydrogels (soft, medium, and stiff formulations), C7 RGD alone, or Hanks' balanced salt solution (HBSS; saline) and loaded into a 10-μl Hamilton syringe. Cells were injected using the same in vivo injection parameters (33-gauge Hamilton syringe needle, 500 nl/min, 4-min rest) into a 24-well plate with 0.5 ml of SC media. After 30 min, cell viability was assessed by LIVE/DEAD staining (Life Technologies) following the manufacturer's instructions and imaged on a Leica SPE confocal microscope.

Biochemical analysis of SC proliferation, spreading, and phenotype

For proliferation assays, SCs were lifted by trypsinization, pelleted, resuspended, and counted. SCs were pelleted again and resuspended in the 10% (w/v) C7 solution to achieve an initial cell seeding density of 1.5×10^7 cells ml^{-1} in the final hydrogels. This cell density was selected to facilitate quantitative image analysis after 3 to 7 days of in vitro culture. Cell-containing C7 was mixed with PEG-P and/or PEG-P-PNIPAM at appropriate gel-forming ratios and transferred to 4 mm (D) × 2.5 mm (H) silicone molds, covered with SC media, and incubated at 37°C. After 3 and 7 days, media were removed, lysis buffer [20 mM tris-HCl, 150 mM NaCl, and 0.5% Triton X-100 (pH 7.4)] was added, and the gels were disrupted by agitation. DNA content was determined using the Quant-iT PicoGreen dsDNA Assay Kit (Life Technologies), following the manufacturer's instructions. Cytotoxicity at 3 and 7 days was also assessed by LIVE/DEAD staining and imaged on a Leica SPE confocal microscope.

For immunocytochemistry, SC-containing hydrogels were fixed with 4% paraformaldehyde in PBS at 37°C for 30 min. Samples were permeabilized with PBS and 0.02% Triton X-100 (PBST) for 1 hour at room temperature and blocked with 5% bovine serum albumin and 10% goat serum (GS) in PBST for 1 hour at room temperature. The samples were then incubated with primary antibodies (rabbit P75 and mouse S100) diluted in PBST with 1% GS overnight at 4°C. Samples were thoroughly washed with PBST and then incubated with Alexa Fluor–conjugated secondary antibodies [AF488 goat anti-mouse, AF546 goat anti-rabbit (Life Technologies), or AF647 goat anti-rabbit (Life Technologies)] and 4′,6-diamidino-2-phenylindole dihydrochloride (DAPI) as a nuclear counterstain for 4 hours at room temperature. For SC actin imaging, cells were incubated with fluorescein isothiocyanate–phalloidin (1:1000; Sigma) and DAPI (1:500; Sigma) for 4 hours at room temperature after immunostaining. Samples were washed thoroughly with PBST and mounted using VECTASHIELD HardSet Antifade Mounting Medium (Vector Laboratories). Samples were imaged using a Leica SPE confocal microscope.

Cervical SCI animal model
Induction of cervical contusion SCI in rats

This protocol was approved by the Stanford Administrative Panel on Laboratory Animal Care. The NIH guidelines for the care and use of laboratory animals were observed (NIH publication no. 85–23 Rev. 1985). Female Fischer 344 rats were used as animal models to determine the efficacy of delivering SCs within SHIELD for functional recovery after SCI. Numbers of animals per group were between 4 and 5 for 48 hours and between 8 and 10 for 4 weeks after transplantation based on (i) power analysis study to determine experimental numbers in animal models of SCIs to appropriately assess statistical differences and (ii) previous publications from the laboratory (table S2) (12). Transplantation studies were completed in two separate, independent studies to demonstrate reproducibility. Before surgery, animals were anesthetized with 1 to 3% isoflurane in oxygen, shaved around the neck and back region, and aseptically prepared with 70% ethanol and betadine solution. Lacri-lube Opthalmic Ointment was applied to the eyes to prevent drying, and the antibiotic penicillin was administered at 115 mU/kg at surgery for the subsequent 3 days. Analgesia (buprenorphine HCl, 0.14 mg/kg) was administered in saline by subcutaneous injection immediately after induction of anesthesia. During surgery, animals were kept on a heating pad to keep their body temperature as close to 37°C as possible. All surgical equipment was sterilized by autoclaving for the first procedure, and for subsequent animals, all surgical equipment used was sterilized in a hot bead sterilizer. Incisions were made to the skin at the area around vertebral level C5, with the smallest incision possible to expose the cord. Muscle layers were separated using forceps to access the vertebra from C4-C6. A laminectomy was performed at the C5 vertebral level, with dura remaining intact, and the spinal column was stabilized with clamps. An Infinite Horizon (IH) device was used to provide a mild 75-kdyne contusion injury (32, 38). The IH impactor was positioned, calibrated over the right side of the exposed C5 spinal cord segment, and triggered to cause the unilateral cervical injury. Subsequently, the muscles were closed in layers (three stitches, double knot) using absorbable Vicryl-coated braided sutures size 5, and the skin incision was closed using clips. Subcutaneous saline was administered to prevent dehydration and normalize blood pressure. Clips will be removed once the wound has healed, usually between days 7 and 10 after injury.

Transplantation of SCs

On day 14 after injury, the same surgery was performed on all rats (as described above) to expose the contusion in the spinal cord. Rats were randomized into one of the following treatment groups: (i) injury

only, (ii) saline only, (iii) SCs in saline, and (iv) SCs in SHIELD. Treatments were injected into the contusion site after bleeding has stopped. SCs were injected at 10×10^7 cells ml^{-1} in a total volume of 4 µl of HBSS (saline) or SHIELD using a 33-gauge needle attached to a 10-µl Hamilton syringe, resulting in a final cell dosage of 4.5×10^5 cells, which is similar to previously published SC transplantation protocols (8, 12). Injections were performed using a microinjection apparatus (KOPF 995 stereotaxic apparatus and Stoelting Co, Quintessential Sterotaxic Injector) at a rate of 500 nl/min for more than 8 min. Saline only control injections were performed exactly as SC injections, with only 4 µl of HBSS. Syringes were left in place for 4 min to minimize reflux after needle withdrawal. Afterward, the incision was closed in layers as described above, and subcutaneous saline was administered to prevent dehydration and normalize blood pressure. Following surgery, rats are returned to a new, clean cage with prewarmed paper towels.

Tissue analysis and immunohistochemistry

Forty-eight hours or 4 weeks after SC transplantation, rats were terminally anesthetized using an intraperitoneal injection of euthanasia solution (sodium pentobarbital, Vedco) and perfused intracardially with approximately 200 to 300 ml of PBS followed by 200 to 300 ml of 4% buffered paraformaldehyde (PFA) solution. The perfusions were performed on the same day for all groups with the same fixative batch. Spinal cords were immediately explanted and post-fixed in PFA overnight at 4°C. After fixation, cords were placed in 30% (w/v in PBS) sucrose overnight at 4°C and then embedded in 10% (w/v in PBS) porcine gelatin (Sigma) blocks. Gelatin-embedded cords were then post-fixed with 4% PFA and placed in 30% sucrose overnight again. Tissue blocks were sectioned into 60-µm sections using a freezing sledge microtome and stored in PBS until use.

Immunostaining of spinal cord explants was carried out between each of the groups, reducing differences in staining between days and groups. One in six sections from each spinal cord was analyzed for transplanted cell number, cystic cavitation, and endogenous secondary injury markers. Tissue sections were immunostained free-floating with mouse monoclonal or rabbit polyclonal antibodies. Sections were blocked with phosphate buffer containing 10% normal donkey serum and 0.2% (v/v) Triton X-100 for 1 hour at room temperature with shaking and then incubated for 48 hours at 4°C in primary antibody diluted in blocking buffer. Mouse monoclonal antibodies used were (i) GFAP (1:500; Sigma) to identify astrocytes and unmyelinated SCs, (ii) Tuj1 (1:500; BioLegend) to stain for spared and regenerated axons, and (iii) ED1 (1:500; Bio-Rad, AbD Serotec) to stain for (hematogenous not resident) pan-macrophages. Rabbit polyclonal antibodies were used for (i) p75 (1:400; Promega, Madison, WI) and (ii) Iba1 (1:500; Wako) to stain for microglia and macrophages. DyLight 488–conjugated Tomato lectin stain (1:100; Vector Laboratories) was used to stain for blood vessels and microglia. Following primary antibody staining, sections were washed three times with PBS and incubated with the appropriate secondary antibodies (donkey anti-rabbit and donkey anti-mouse, 1:400 in blocking buffer, Jackson ImmunoLabs) for 4 hours at room temperature. Last, sections were washed three times in PBS, mounted onto glass slides, and mounted in Diamond ProLong Gold Antifade mounting medium (Life Technologies) with DAPI. Low-magnification (×10 objective) fluorescent images were taken using an IX70 Olympus microscope, and higher-magnification images (×20 and ×40) were taken using Leica SPE confocal microscope.

Analysis of cystic cavitation volume, cell survival, morphology and distribution, and endogenous marker expression in vivo

Tissue cavitation was measured in all animals to evaluate the effect of the transplanted SCs upon the secondary injury response and preservation of tissue at the lesion site. The combined area of any cystic cavities (including areas showing signs of degeneration, such as microcysts) throughout the serial cord was measured using ImageJ (34) from 4-week post-transplantation GFAP-stained tissue sections and multiplied by section thickness (60 µm) to obtain an estimation of cavitation volume.

For calculation of transplanted SC retention, the total number of observed P75$^+$ cells was manually counted using ImageJ in 48-hour and 4-week explanted sections, summed together, and multiplied by 6 (one of six serial sections). SC spindle ratio was determined by measuring the major and minor axis lengths of P75$^+$ cells with clearly defined borders at the injection epicenter for all animals. SC distribution along the length of the cord and SCI lesion was determined by counting the number of P75$^+$ cells at selected cross sections at the specified locations along the cord (1:6 stained serial sections, 60 µm thick). To establish that P75$^+$ cells were the result of transplantation and not endogenous migrating SCs, a subset of animals were transplanted with SC labeled with Qtracker655 (Invitrogen) using the manufacturer's protocols (fig. S9). In vitro monitoring of Qtracker655-labeled cells confirmed coexpression of label and P75 for up to 4 weeks in vitro. In vivo, Qtracker655-labeled cells colocalized with P75$^+$ cells at both 48 hours and 4 weeks after transplantation.

To evaluate the impact of SC retention on the expression of secondary injury response markers, one of six serial, 4-week post-transplantation sections were stained with GFAP (astrocytes), ED1 (pan-macrophages), Iba1 (microglia), and Tomato lectin (blood vessels and microglia). Tile scans of whole sections were taken at ×20 magnification. Percent positive stained pixel area was measured using ImageJ in two regions of the sections: (i) the 100-µm region adjacent to the cavity, defined as the lesion, and (ii) the subsequent 100-µm region, defined as the peri-lesion (34).

Forelimb behavioral assessments
Grip strength for behavioral assessment

Forelimb grip strength tests were performed on the animals before injury, after injury, and then weekly throughout the experimental timeline (4 weeks) to evaluate functional improvement of their forelimbs. For this test, animals were allowed to preferentially grip the handle bars of the grip strength machine (TSE Systems, 303500 Series) and pulled back until they let go of the bars, and the force with which they held on was recorded. This was repeated six times, for both forelimbs and right forelimb only, upon which the lowest and highest values were dropped and the remaining four values were averaged together.

Horizontal Ladder Walk for behavioral assessment

Horizontal Ladder Walk tests were performed on the animals before injury, after injury, and then weekly throughout the experimental timeline (4 weeks) to evaluate functional improvement of their forelimb coordination. For this test, animals were placed within a Plexiglas alleyway with metal rungs placed between 1 and 3 cm apart for varying difficulty. Animals were recorded (Sony HDR-CX675 camera) walking across the rungs, and the number of correct and incorrect (slipped and misplaced) forearm steps was recorded by blinded observers. The percentage of missed steps was calculated

by dividing the number of incorrect steps by the total (correct and incorrect steps) number of steps and multiplying the quotient by 100.

Statistical analysis

All data are presented as mean ± SEM, and statistical analysis was performed using GraphPad Prism software. Statistical comparisons on shear moduli, cell viability, DNA content, SC cluster area, and SC process length were performed by one-way analysis of variance (ANOVA) with Tukey post hoc test. One-way ANOVA with Tukey post hoc test was performed on in vivo SC number and endogenous marker immunostaining and functional behavior results. Statistical comparisons were performed by unpaired, two-tailed t test with Welch's correction for in vivo SC spindle ratio. Statistical comparisons were performed by one-way ANOVA with unpaired, two-tailed t test for in vivo cystic cavitation. Correlations between measurements (transplanted SC count at 4 weeks, lesion volume, combined grip strength, right forelimb grip strength, and percentage of missed steps in horizontal ladder assay) were performed with a two-tailed Pearson correlation test with 95% confidence interval. Last, statistical comparisons were performed on in vivo SC distribution in the spinal cord by nonparametric Kolmogorov-Smirnov test for cumulative distribution analysis. Values were considered to be significantly different when the P value was less than 0.05.

SUPPLEMENTARY MATERIALS

Supplementary material for this article is available at http://advances.sciencemag.org/cgi/content/full/6/14/eaaz1039/DC1

View/request a protocol for this paper from *Bio-protocol*.

REFERENCES AND NOTES

1. M. B. Bunge, D. D. Pearse, Transplantation strategies to promote repair of the injured spinal cord. *J. Rehabil. Res. Dev.* **40**, (4 suppl. 1) 55–62 (2003).
2. K. D. Anderson, J. D. Guest, W. D. Dietrich, M. Bartlett Bunge, R. Curiel, M. Dididze, B. A. Green, A. Khan, D. D. Pearse, E. Saraf-Lavi, E. Widerström-Noga, P. Wood, A. D. Levi, Safety of autologous human Schwann cell transplantation in subacute thoracic spinal cord injury. *J. Neurotrauma* **34**, 2950–2963 (2017).
3. M. B. Bunge, P. V. Monje, A. Khan, P. M. Wood, From transplanting Schwann cells in experimental rat spinal cord injury to their transplantation into human injured spinal cord in clinical trials. *Prog. Brain Res.* **231**, 107–133 (2017).
4. J. Guest, A. J. Santamaria, F. D. Benavides, Clinical translation of autologous Schwann cell transplantation for the treatment of spinal cord injury. *Curr. Opin. Organ Transplant.* **18**, 682–689 (2013).
5. M. B. Bunge, P. M. Wood, Realizing the maximum potential of Schwann cells to promote recovery from spinal cord injury. *Handb. Clin. Neurol.* **109**, 523–540 (2012).
6. R.-J. Swijnenburg, S. Schrepfer, J. A. Govaert, F. Cao, K. Ransohoff, A. Y. Sheikh, M. Haddad, A. J. Connolly, M. M. Davis, R. C. Robbins, J. C. Wu, Immunosuppressive therapy mitigates immunological rejection of human embryonic stem cell xenografts. *Proc. Natl. Acad. Sci. U.S.A.* **105**, 12991–12996 (2008).
7. M. H. Amer, F. Rose, K. M. Shakesheff, M. Modo, L. J. White, Translational considerations in injectable cell-based therapeutics for neurological applications: Concepts, progress and challenges. *NPJ Regen Med* **2**, 23 (2017).
8. C. E. Hill, A. Hurtado, B. Blits, B. A. Bahr, P. M. Wood, M. Bartlett Bunge, M. Oudega, Early necrosis and apoptosis of Schwann cells transplanted into the injured rat spinal cord. *Eur. J. Neurosci.* **26**, 1433–1445 (2007).
9. B. A. Aguado, W. Mulyasasmita, J. Su, K. J. Lampe, S. C. Heilshorn, Improving viability of stem cells during syringe needle flow through the design of hydrogel cell carriers. *Tissue Eng. Part A* **18**, 806–815 (2012).
10. J. D. Glass, N. M. Boulis, K. Johe, S. B. Rutkove, T. Federici, M. Polak, C. Kelly, E. L. Feldman, Lumbar intraspinal injection of neural stem cells in patients with amyotrophic lateral sclerosis: Results of a phase I trial in 12 patients. *Stem Cells* **30**, 1144–1151 (2012).
11. C. E. Hill, Y. Guller, S. J. Raffa, A. Hurtado, M. B. Bunge, A calpain inhibitor enhances the survival of schwann cells in vitro and after transplantation into the injured spinal cord. *J. Neurotrauma* **27**, 1685–1695 (2010).
12. H. R. Barbour, C. D. Plant, A. R. Harvey, G. W. Plant, Tissue sparing, behavioral recovery, supraspinal axonal sparing/regeneration following sub-acute glial transplantation in a model of spinal cord contusion. *BMC Neurosci.* **14**, 106 (2013).
13. V. Patel, G. Joseph, A. Patel, S. Patel, D. Bustin, D. Mawson, L. M. Tuesta, R. Puentes, M. Ghosh, D. D. Pearse, Suspension matrices for improved Schwann-cell survival after implantation into the injured rat spinal cord. *J. Neurotrauma* **27**, 789–801 (2010).
14. M. Koda, Y. Someya, Y. Nishio, R. Kadota, C. Mannoji, T. Miyashita, A. Okawa, A. Murata, M. Yamazaki, Brain-derived neurotrophic factor suppresses anoikis-induced death of Schwann cells. *Neurosci. Lett.* **444**, 143–147 (2008).
15. L. Cai, R. E. Dewi, S. C. Heilshorn, Injectable hydrogels with in situ double network formation enhance retention of transplanted stem cells. *Adv. Funct. Mater.* **25**, 1344–1351 (2015).
16. C. Yan, M. E. Mackay, K. Czymmek, R. P. Nagarkar, J. P. Schneider, D. J. Pochan, Injectable solid peptide hydrogel as a cell carrier: Effects of shear flow on hydrogels and cell payload. *Langmuir* **28**, 6076–6087 (2012).
17. L. M. Marquardt, S. C. Heilshorn, Design of injectable materials to improve stem cell transplantation. *Curr. Stem Cell Rep.* **2**, 207–220 (2016).
18. T. P. Martens, A. F. G. Godier, J. J. Parks, L. Q. Wan, M. S. Koeckert, G. M. Eng, B. I. Hudson, W. Sherman, G. Vunjak-Novakovic, Percutaneous cell delivery into the heart using hydrogels polymerizing in situ. *Cell Transplant.* **18**, 297–304 (2009).
19. C. B. Rodell, M. E. Lee, H. Wang, S. Takebayashi, T. Takayama, T. Kawamura, J. S. Arkles, N. N. Dusaj, S. M. Dorsey, W. R. T. Witschey, J. J. Pilla, J. H. Gorman III, J. F. Wenk, J. A. Burdick, R. C. Gorman, Injectable shear-thinning hydrogels for minimally invasive delivery to infarcted myocardium to limit left ventricular remodeling. *Circ. Cardiovasc. Interv.* **9**, e004058 (2016).
20. W. P. Russ, D. M. Lowery, P. Mishra, M. B. Yaffe, R. Ranganathan, Natural-like function in artificial WW domains. *Nature* **437**, 579–583 (2005).
21. C. T. Wong Po Foo, J. S. Lee, W. Mulyasasmita, A. Parisi-Amon, S. C. Heilshorn, Two-component protein-engineered physical hydrogels for cell encapsulation. *Proc. Natl. Acad. Sci. U.S.A.* **106**, 22067–22072 (2009).
22. E. Moeendarbary, I. P. Weber, G. K. Sheridan, D. E. Koser, S. Soleman, B. Haenzi, E. J. Bradbury, J. Fawcett, K. Franze, The soft mechanical signature of glial scars in the central nervous system. *Nat. Commun.* **8**, 14787 (2017).
23. N. H. Romano, C. M. Madl, S. C. Heilshorn, Matrix RGD ligand density and L1CAM-mediated Schwann cell interactions synergistically enhance neurite outgrowth. *Acta Biomater.* **11**, 48–57 (2015).
24. S. Suri, C. E. Schmidt, Cell-laden hydrogel constructs of hyaluronic acid, collagen, and laminin for neural tissue engineering. *Tissue Eng. Part A* **16**, 1703–1716 (2010).
25. Y. Wang, H.-L. Teng, Z.-h. Huang, Intrinsic migratory properties of cultured Schwann cells based on single-cell migration assay. *PLOS ONE* **7**, e51824 (2012).
26. Y. Wang, Q. Shan, J. Pan, S. Yi, Actin cytoskeleton affects Schwann cell migration and peripheral nerve regeneration. *Front. Physiol.* **9**, 23 (2018).
27. A. Farrukh, F. Ortega, W. Fan, N. Marichal, J. I. Paez, B. Berninger, A. del Campo, M. J. Salierno, Bifunctional hydrogels containing the laminin motif IKVAV promote neurogenesis. *Stem Cell Rep.* **9**, 1432–1440 (2017).
28. S. P. Massia, S. S. Rao, J. A. Hubbell, Covalently immobilized laminin peptide Tyr-Ile-Gly-Ser-Arg (YIGSR) supports cell spreading and co-localization of the 67-kilodalton laminin receptor with alpha-actinin and vinculin. *J. Biol. Chem.* **268**, 8053–8059 (1993).
29. L. Cai, R. E. Dewi, A. B. Goldstone, J. E. Cohen, A. N. Steele, Y. J. Woo, S. C. Heilshorn, Regulating stem cell secretome using injectable hydrogels with in situ network formation. *Adv. Healthc. Mater.* **5**, 2758–2764 (2016).
30. W. Mulyasasmita, L. Cai, R. E. Dewi, A. Jha, S. D. Ullmann, R. H. Luong, N. F. Huang, S. C. Heilshorn, Avidity-controlled hydrogels for injectable co-delivery of induced pluripotent stem cell-derived endothelial cells and growth factors. *J. Control. Release* **191**, 71–81 (2014).
31. Y. Gu, Y. Ji, Y. Zhao, Y. Liu, F. Ding, X. Gu, Y. Yang, The influence of substrate stiffness on the behavior and functions of Schwann cells in culture. *Biomaterials* **33**, 6672–6681 (2012).
32. A. R. Ferguson, K.-A. Irvine, J. C. Gensel, J. L. Nielson, A. Lin, J. Ly, M. R. Segal, R. R. Ratan, J. C. Bresnahan, M. S. Beattie, Derivation of multivariate syndromic outcome metrics for consistent testing across multiple models of cervical spinal cord injury in rats. *PLOS ONE* **8**, e59712 (2013).
33. G. W. Plant, C. L. Christensen, M. Oudega, M. B. Bunge, Delayed transplantation of olfactory ensheathing glia promotes sparing/regeneration of supraspinal axons in the contused adult rat spinal cord. *J. Neurotrauma* **20**, 1–16 (2003).
34. L. R. Nih, S. Gojgini, S. T. Carmichael, T. Segura, Dual-function injectable angiogenic biomaterial for the repair of brain tissue following stroke. *Nat. Mater.* **17**, 642–651 (2018).
35. G. K. Tofaris, P. H. Patterson, K. R. Jessen, R. Mirsky, Denervated Schwann cells attract macrophages by secretion of leukemia inhibitory factor (LIF) and monocyte chemoattractant protein-1 in a process regulated by interleukin-6 and LIF. *J. Neurosci.* **22**, 6696–6703 (2002).

36. D. J. Donnelly, P. G. Popovich, Inflammation and its role in neuroprotection, axonal regeneration and functional recovery after spinal cord injury. *Exp. Neurol.* **209**, 378–388 (2008).

37. O. N. Hausmann, Post-traumatic inflammation following spinal cord injury. *Spinal Cord* **41**, 369–378 (2003).

38. J. C. Gensel, C. A. Tovar, F. P. T. Hamers, R. J. Deibert, M. S. Beattie, J. C. Bresnahan, Behavioral and histological characterization of unilateral cervical spinal cord contusion injury in rats. *J. Neurotrauma* **23**, 36–54 (2006).

39. K. D. Anderson, M. Abdul, O. Steward, Quantitative assessment of deficits and recovery of forelimb motor function after cervical spinal cord injury in mice. *Exp. Neurol.* **190**, 184–191 (2004).

40. S. M. Onifer, J. F. Rodríguez, D. I. Santiago, J. C. Benitez, D. T. Kim, J. P. R. Brunschwig, J. T. Pacheco, J. V. Perrone, O. Llorente, D. H. Hesse, A. Martinez-Arizala, Cervical spinal cord injury in the adult rat: Assessment of forelimb dysfunction. *Restor. Neurol. Neurosci.* **11**, 211–223 (1997).

41. I. Antonow-Schlorke, J. Ehrhardt, M. Knieling, Modification of the ladder rung walking task—New options for analysis of skilled movements. *Stroke Res. Treat.* **2013**, 418627 (2013).

42. A. A. Foster, R. E. Dewi, L. Cai, L. Hou, Z. Strassberg, C. A. Alcazar, S. C. Heilshorn, N. F. Huang, Protein-engineered hydrogels enhance the survival of induced pluripotent stem cell–derived endothelial cells for treatment of peripheral arterial disease. *Biomater. Sci.* **6**, 614–622 (2018).

43. T. E. Robey, M. K. Saiget, H. Reinecke, C. E. Murry, Systems approaches to preventing transplanted cell death in cardiac repair. *J. Mol. Cell. Cardiol.* **45**, 567–581 (2008).

44. M. J. Caicco, T. Zahir, A. J. Mothe, B. G. Ballios, A. J. Kihm, C. H. Tator, M. S. Shoichet, Characterization of hyaluronan-methylcellulose hydrogels for cell delivery to the injured spinal cord. *J. Biomed. Mater. Res. A* **101**, 1472–1477 (2013).

45. K. M. Piltti, S. N. Avakian, G. M. Funes, A. Hu, N. Uchida, A. J. Anderson, B. J. Cummings, Transplantation dose alters the dynamics of human neural stem cell engraftment, proliferation and migration after spinal cord injury. *Stem Cell Res.* **15**, 341–353 (2015).

46. N. Rao, G. Agmon, M. T. Tierney, J. L. Ungerleider, R. L. Braden, A. Sacco, K. L. Christman, Engineering an injectable muscle-specific microenvironment for improved cell delivery using a nanofibrous extracellular matrix hydrogel. *ACS Nano* **11**, 3851–3859 (2017).

47. G. Flora, G. Joseph, S. Patel, A. Singh, D. Bleicher, D. J. Barakat, J. Louro, S. Fenton, M. Garg, M. B. Bunge, D. D. Pearse, Combining neurotrophin-transduced schwann cells and rolipram to promote functional recovery from subacute spinal cord injury. *Cell Transplant.* **22**, 2203–2217 (2013).

48. J. Robinson, P. Lu, Optimization of trophic support for neural stem cell grafts in sites of spinal cord injury. *Exp. Neurol.* **291**, 87–97 (2017).

49. X. Ee, Y. Yan, D. A. Hunter, L. Schellhardt, S. E. Sakiyama-Elbert, S. E. Mackinnon, M. D. Wood, Transgenic SCs expressing GDNF-IRES-DsRed impair nerve regeneration within acellular nerve allografts. *Biotechnol. Bioeng.* **114**, 2121–2130 (2017).

50. R. Eggers, F. de Winter, S. A. Hoyng, K. C. D. Roet, E. M. Ehlert, M. J. A. Malessy, J. Verhaagen, M. R. Tannemaat, Lentiviral vector-mediated gradients of GDNF in the injured peripheral nerve: Effects on nerve coil formation, schwann cell maturation and myelination. *PLOS ONE* **8**, e71076 (2013).

51. L. M. Marquardt, X. Ee, N. Iyer, D. Hunter, S. E. Mackinnon, M. D. Wood, S. E. Sakiyama-Elbert, Finely tuned temporal and spatial delivery of GDNF promotes enhanced nerve regeneration in a long nerve defect model. *Tissue Eng. Part A* **21**, 2852–2864 (2015).

52. Y. S. Lee, S. Wu, T. L. Arinzeh, M. B. Bunge, Transplantation of schwann cells inside PVDF-TrFE conduits to bridge transected rat spinal cord stumps to promote axon regeneration across the gap. *J. Vis. Exp.* **2017**, e56077 (2017).

53. M. Uemura, M. M. Refaat, M. Shinoyama, H. Hayashi, N. Hashimoto, J. Takahashi, Matrigel supports survival and neuronal differentiation of grafted embryonic stem cell–derived neural precursor cells. *J. Neurosci. Res.* **88**, 542–551 (2010).

54. S. R. Cerqueira, Y.-S. Lee, R. C. Cornelison, M. W. Mertz, R. A. Wachs, C. E. Schmidt, M. B. Bunge, Decellularized peripheral nerve supports Schwann cell transplants and axon growth following spinal cord injury. *Biomaterials* **177**, 176–185 (2018).

55. J. A. Gomez-Sanchez, K. S. Pilch, M. van der Lans, S. V. Fazal, C. Benito, L. J. Wagstaff, R. Mirsky, K. R. Jessen, After nerve injury, lineage tracing shows that myelin and Remak Schwann cells elongate extensively and branch to form repair schwann cells, which shorten radically on remyelination, which shorten radically on remyelination. *J. Neurosci.* **37**, 9086–9099 (2017).

56. J. Lam, S. T. Carmichael, W. E. Lowry, T. Segura, Hydrogel design of experiments methodology to optimize hydrogel for iPSC-NPC culture. *Adv. Healthc. Mater.* **4**, 534–539 (2015).

57. J. P. Jung, J. V. Moyano, J. H. Collier, Multifactorial optimization of endothelial cell growth using modular synthetic extracellular matrices. *Integr. Biol.* **3**, 185–196 (2011).

58. M. M. Pakulska, B. G. Ballios, M. S. Shoichet, Injectable hydrogels for central nervous system therapy. *Biomed. Mater.* **7**, 024101 (2012).

59. D. Gupta, C. H. Tator, M. S. Shoichet, Fast-gelling injectable blend of hyaluronan and methylcellulose for intrathecal, localized delivery to the injured spinal cord. *Biomaterials* **27**, 2370–2379 (2006).

60. Y. Aida, M. J. Pabst, Removal of endotoxin from protein solutions by phase separation using Triton X-114. *J. Immunol. Methods* **132**, 191–195 (1990).

Citation: L. M. Marquardt, V. M. Doulames, A. T. Wang, K. Dubbin, R. A. Suhar, M. J. Kratochvil, Z. A. Medress, G. W. Plant, S. C. Heilshorn, Designer, injectable gels to prevent transplanted Schwann cell loss during spinal cord injury therapy. *Sci. Adv.* **6**, eaaz1039 (2020).

Designer, injectable gels to prevent transplanted Schwann cell loss during spinal cord injury therapy

Laura M. Marquardt, Vanessa M. Doulames, Alice T. Wang, Karen Dubbin, Riley A. Suhar, Michael J. Kratochvil, Zachary A. Medress, Giles W. Plant and Sarah C. Heilshorn

ARTICLE TOOLS	http://advances.sciencemag.org/content/6/14/eaaz1039
SUPPLEMENTARY MATERIALS	http://advances.sciencemag.org/content/suppl/2020/03/30/6.14.eaaz1039.DC1
REFERENCES	This article cites 60 articles, 6 of which you can access for free http://advances.sciencemag.org/content/6/14/eaaz1039#BIBL
PERMISSIONS	http://www.sciencemag.org/help/reprints-and-permissions

Use of this article is subject to the Terms of Service